Detection of Prenatal Alcohol Exposure Using Machine Learning Classification of Resting-State Functional Network Connectivity Data

Carlos I. Rodriguez, Ph.D.[1], Victor Vergara, Ph.D.[2], Suzy Davies, Ph.D.[3], Vince Calhoun, Ph.D.[2,1] Daniel D. Savage, Ph.D.[3,4], Derek A. Hamilton, Ph.D.[3,4]

Affiliations

1. The Mind Research Network. 1101 Yale Blvd. NE, Albuquerque, NM, 87106, USA.
2. Tri-Institutional Center for Translational Research in Neuroimaging and Data Science (TReNDS), Georgia State University, Georgia Institute of Technology, and Emory University. 55 Park Pl NE, Atlanta, GA 30303, USA.
3. Dept. of Neurosciences, University of New Mexico School of Medicine. 1 University of New Mexico, Albuquerque, NM, 87131, USA.
4. Department of Psychology, University of New Mexico. 1 University of New Mexico, Albuquerque, NM 87131, USA.

Running Title: Classification of Prenatal Alcohol Exposure

***Corresponding Author**:*

Carlos I. Rodriguez

The Mind Research Network

1101 Yale Boulevard Northeast

Albuquerque, NM 87106

Phone: 505-301-5483

Email: crodriguez@mrn.org

Keywords: Prenatal Alcohol Exposure, Fetal Alcohol Spectrum Disorder, Machine Learning, Functional Network Connectivity

ABSTRACT

Introduction: Previous work utilizing resting state fMRI to measure functional network connectivity in rodents with moderate prenatal alcohol exposure (PAE) revealed several sex- and region-dependent alterations in FNC implicating FNC as potential biomarker for PAE. Given that FNC is sensitive to neurological and psychiatric conditions in humans, here, we explore the use of previously acquired FNC data and machine learning methods to detect PAE among a sample of rodents exposed to moderate PAE and controls exposed to a saccharin solution.

Materials & Methods: We utilized previously acquired fMRI data from 48 adult rats 24 PAE (12 male 12 female) and 24 saccharin exposed (SAC) controls (12 male and 12 female) for classification. The entire data sample was utilized to perform binary classification (SAC or PAE) of FNC data with multiple support vector machine (SVM) kernels and out-of-sample cross-validation to evaluate classification performance.

Results: Results revealed accuracy rates of 62.5% for all samples, 58.3% for males, and 79.2% for females using a quadratic SVM kernel to classify moderate PAE from FNC data. In addition, brain networks localized to hippocampal and cortical regions contributed strongly to QSVM classifications.

Conclusion: Our results suggest overall modest classification performance of a QSVM to detect moderate PAE from FNC data gathered from adult rats, yet good performance among females. Further developments and refinement of the technique hold promise for the detection of PAE in earlier developmental time periods that potentially offer additional tools for the non-invasive detection of PAE from FNC data.

IMPACT STATEMENT

The diagnosis of fetal alcohol spectrum disorders (FASDs) can be challenging in individuals who lack the hallmark facial dysmorphologies associated with heavy prenatal alcohol exposure (PAE). The absence of a diagnosis prevents individuals with PAE from receiving the treatment and services that improves quality of life outcomes. This research explores the use of preclinical functional network connectivity data and machine learning techniques as a novel and non-invasive means of detecting PAE. Our aim is to contribute basic science towards improving diagnostic strategies that can lead to securing timely and appropriate support for individuals with FASD and their caregivers.

ACRONYMS

BOLD	Blood Oxygen Level Dependent
FAS	Fetal Alcohol Syndrom
FASD	Fetal Alcohol Spectrum Disorder
fMRI	function Magnetic Resonance Imaging
FNC	Functional Network Connectivity
FWHM	Full Width Half Max
GICA	Group Independent Components Analysis
GIFT	Group ICA of fMRI Toolbox
HPA	Hypothalamic Pituitary Adrenal Axis
LOOCV	Leave One Out Cross Validation
MLP	Multilayer Perceptron
mTBI	mild Traumatic Brain Injury
NMDA	N-methyl-D-Aspartate
PAE	Prenatal Alcohol Exposure
QSVM	Quadratic SVM
RBF	Radial Basis Function
RSN	Resting State Network
SAC	Saccharin
SVM	Support Vector Machine

INTRODUCTION

Fetal alcohol spectrum disorder (FASD) is a term that is utilized to encompass a wide range of morphological and neuro-behavioral phenotypes caused by exposure to alcohol during prenatal development (Loock, Conry, Cook, Chudley, & Rosales, 2005; Williams, Smith, & Committee On Substance, 2015). The most severe end of the spectrum is known as Fetal Alcohol Syndrome (FAS) and is linked to heavy prenatal alcohol exposure (PAE) (Lemoine, Harousseau, Borteyru, & Menuet, 1968; Manning & Eugene Hoyme, 2007). Children with FAS exhibit facial dysmorphologies, growth deficits, and numerous impairments in cognitive and behavioral functions related to attention, learning, memory, and motor coordination among others (Connor, Sampson, Bookstein, Barr, & Streissguth, 2000; Jones & Smith, 1973, 1975; Streissguth et al., 1986). Although the most severe, FAS is the least common with an estimated prevalence rate of ~0.1% in the U.S. (May & Gossage, 2001). However, when considering the entire spectrum, estimated prevalence rates of FASD (including FAS) fall between 1.1% and 5.0% of U.S. children, many of which will not display readily identifiable facial dysmorphologies, but may nonetheless exhibit cognitive and behavioral deficits (May et al., 2014; May et al., 2018). Unfortunately, children who do not display the facial dysmorphologies characteristic of FAS, due to lack of early diagnosis, may not receive timely treatment or services, negatively impacting life outcomes related to academic success (Mattson & Riley, 1998), difficulty finding and maintaining meaningful employment, and staying out of trouble with the law (Popova, Stade, Bekmuradov, Lange, & Rehm, 2011).

From the early clinical descriptions of FAS (Jones & Smith, 1973, 1975), research with human participants has been critical for understanding the social, physical, and neuro-behavioral sequelae of PAE (Connor et al., 2000; Streissguth et al., 2004). However, variables such as dose (e.g., high, moderate, low), timing (e.g., 1st, 2nd trimester), and pattern of alcohol exposure (e.g., daily vs binge), can be difficult to account for and, for ethical reasons, are impossible to experimentally manipulate in human subjects research (Patten, Fontaine, & Christie, 2014). To overcome these challenges, animal models of FASD have been important for illuminating the underlying neurobiological consequences associated with developmental alcohol exposure.

Given that children are more likely to be exposed to moderate, rather than heavy, levels of prenatal alcohol exposure (May et al., 2018; May & Gossage, 2001), animal research aimed at studying the effects of moderate PAE is extremely valuable because it more closely mimics the pattern of alcohol exposure observed in the human population. Within animal models of PAE, considerable work has been undertaken with the aim of investigating discrete brain areas such as the hippocampus (Gil-Mohapel, Boehme, Kainer, & Christie, 2010; Savage, Becher, de la Torre, & Sutherland, 2002) and cerebellum (Servais et al., 2007). However, higher level cognitive and behavioral functions, including those associated with FASD, involve sophisticated and highly coordinated activity across multiple, rather than single, brain regions (Green et al., 2009). Functional network connectivity (FNC) methods (i.e. functional connectivity between coherent brain networks) offer an important lens that can be leveraged to understand the temporal statistical dependencies (e.g. correlations) of multiple and distant brain networks (Arbabshirani & Calhoun, 2011) following PAE. Functional

magnetic resonance imaging (fMRI), a neuroimaging modality employed to non-invasively measure blood-oxygenation-level dependent (BOLD) signals that reflect patterns of neuronal activity (Logothetis, Pauls, Augath, Trinath, & Oeltermann, 2001; Raichle & Mintun, 2006), has been widely utilized to derive measures of FNC (Allen et al., 2011). Group level fMRI data gathered at rest, an experimental condition that lacks externally presented stimuli or behavioral responses (Snyder & Raichle, 2012), can be examined by group independent component analysis (GICA). As a blind source separation algorithm, GICA is a data driven technique that extracts the temporal activation patterns (time courses) of resting state networks (RSNs) where each network may consist of multiple brain regions (Allen et al., 2011; Arbabshirani & Calhoun, 2011; Buckner, Krienen, & Yeo, 2013). FNC assessment consists of correlations between the time-courses of brain networks. Brain dysfunction can then be identified by abnormal correlations (e.g. too high or too low) when comparing FNC across control and experimental treatment conditions.

Previous work from our group applied GICA to resting state fMRI data acquired from adult rodents exposed to moderate levels of PAE that revealed several sex and regionally dependent alterations in functional network connectivity (Rodriguez, Davies, Calhoun, Savage, & Hamilton, 2016) and point to FNC is a potential biomarker for the identification of PAE. In human-subjects research, measures of FNC from fMRI data have also been successfully utilized to detect patients with schizophrenia and mild traumatic brain injury (mTBI) using machine learning algorithms (Rashid et al., 2016; Vergara, Mayer, Damaraju, Kiehl, & Calhoun, 2017). In this study, we explored the use of multiple binary-classification machine learning algorithms and leave-one-out-cross

validation (LOOCV) to detect PAE among a mixed sample of FNC data from alcohol- and saccharin-exposed (SAC; control) rodents. Functional neuroimaging data were obtained from our previously published report that characterized the effects of moderate PAE on FNC by utilizing GICA of resting-state fMRI data (Rodriguez, Davies, et al., 2016). The primary goal of this current investigation was to explore the utility of machine learning algorithms a novel and non-invasive means to detect aberrant patterns of FNC in a rodent model of FASD.

METHODS

Subjects

Subjects, materials, and procedures were previously reported in separate studies approved by the Institutional Animal Care and Use Committee of the University of New Mexico main campus and Health Sciences Center (Rodriguez, Davies, et al., 2016; Rodriguez, Magcalas, et al., 2016). Briefly, 48 Long-Evans rats (24 SAC and 24 PAE) were generated in a single breeding round designed to prenatally expose rats to either a 5% ethanol (v/v) or 0.066% saccharin solution (Hamilton et al., 2014) for the duration of the entire 21-day gestational period. Following weaning, animals were housed with an age- and weight-matched cagemate from the same prenatal treatment, but different litter, in standard plastic cages with water and food available ad libitum.

At 3-4 months of age, all animals underwent a series of structural- and blood oxygenation level dependent (BOLD) fMRI-scan sequences under isoflurane anesthesia for ~45 min in a 4.7T Bruker Biospin (Billerica, MA) MRI scanner. Functional MRI data were acquired with a 10-minute echo planar imaging acquisition at a temporal resolution

(TR) of 2 sec (FOV = 3.84 cm x 3.84 cm, matrix = 64 x 64, TE = 21.3 ms, flip angle = 90°, 27 slices, and slice thickness = 1 mm).

Image Preprocessing, Group Independent Component Analysis (GICA), and Functional Network Connectivity

Preprocessing, GICA, and FNC methods are described in (Rodriguez, Davies, et al., 2016). To summarize, fMRI data preprocessing included realignment, spatial normalization to the Paxinos & Watson atlas (Schweinhardt, Fransson, Olson, Spenger, & Andersson, 2003), and smoothing with a 0.5 mm full-width-half-maximum (FWHM) Gaussian kernel in Statistical Parametric Mapping 8 (SPM8) (Wellcome Department of Cognitive Neurology, London, UK) running in MATLAB (Mathworks, Inc., Natick, MA) version R2012b. After preprocessing, 40 group-level independent components were extracted utilizing the Infomax algorithm (Bell & Sejnowski, 1995) in the Group ICA of fMRI Toolbox (GIFT, www.trendscenter.org/software/gift) (Calhoun, Adali, Pearlson, & Pekar, 2001). Of the initial 40 components, 17 components were retained based on the exclusion of components localized to white matter tracts or cerebro-spinal fluid and the presence of artifactual features upon visual inspection.

In this study, component time courses were orthogonalized with respect to the following: (1) linear, quadratic, and cubic trends; (2) the six realignment parameters (translation in the x, y, and z directions and rotations about the x, y, z axes); and the 6 realignment parameter derivatives. Time-courses were lowpass filtered with a cutoff at 0.15Hz. Functional network connectivity (FNC) measures were estimated from pairwise correlations between average individual component time-courses for each rat. A total of 136 unique pairwise correlations were calculated for each animal given by the following:

196 $\left(\frac{C*(C-1)}{2}\right)$ where *C* = 17 (the number of retained components). Thus, the structure of the
197 FNC data utilized for machine learning procedures consisted of 48 correlation matrices.
198 All correlation values were Fisher's Z transformed for subsequent analyses.

199 **Machine Learning Procedures**

200 The machine learning methods to classify FNC patterns between PAE and SAC
201 animals was based on work previously described in (Vergara, Mayer, Kiehl, & Calhoun,
202 2018) and relied on utilizing FNC data from GICA-extracted components. SVM tuning
203 parameters included a least squares solving method, a soft margin parameter of 0.1
204 and a feature selection threshold of 0.75. Feature selection is implemented by running a
205 two-sample t-test on SAC and PAE groups for each of the 136 FNC values and
206 discarding FNCs with a t-value failing to meet the t = 0.75 threshold. This SVM
207 configuration was used to run five different SVM Kernels: linear, quadratic (QSVM),
208 cubic, radial basis functions (RBF) and multilayer perceptron (MLP) kernels in MATLAB
209 (Mathworks, Inc., Natick, MA) version 2016b to perform binary classification of FNC
210 data at the subject level. Because of the relatively small sample size, leave-one-out
211 cross validation (LOOCV) was chosen to assess classification performance. The
212 LOOCV procedure consisted of isolating one sample for testing and the remainder of
213 the samples for training across multiple iterations as displayed in Figure 1. Statistical
214 significance was assessed by a permutation test approach in which the prenatal
215 condition labels of individual subject's FNC data were randomized and subsequently
216 subjected to 10,000 replications of QSVM classification and LOOCV with random
217 groups on each replication to establish the null probability distribution of accuracy rates
218 from randomized data (null model). Significance at the p = 0.05 level was estimated

219 from the null distribution. Finally, to address potential differences in sex, the permutation
220 test approach and LOOCV procedures were repeated separately for male and female
221 samples.

222

Figure 1. Leave-one-out cross validation schematic illustrates FNC matrices that represent the 136 pairwise correlations of RSNs (blue=negative correlations, red=positive correlations) for each subject (48). For each iteration, the connectivity matrix from the n^{th} subject is left out (1), the remaining 47 matrices underwent feature selection based on a t-value threshold (2), and then utilized for training the SVM (3). The left out, n^{th}, subject data is then utilized for measuring (4) performing a classification decision (5). Finally, the nth subject data is replaced (6) and the process reiterates until all 48 classification decisions were gathered. Correct classifications out of 48 comprise SVM accuracy rates.

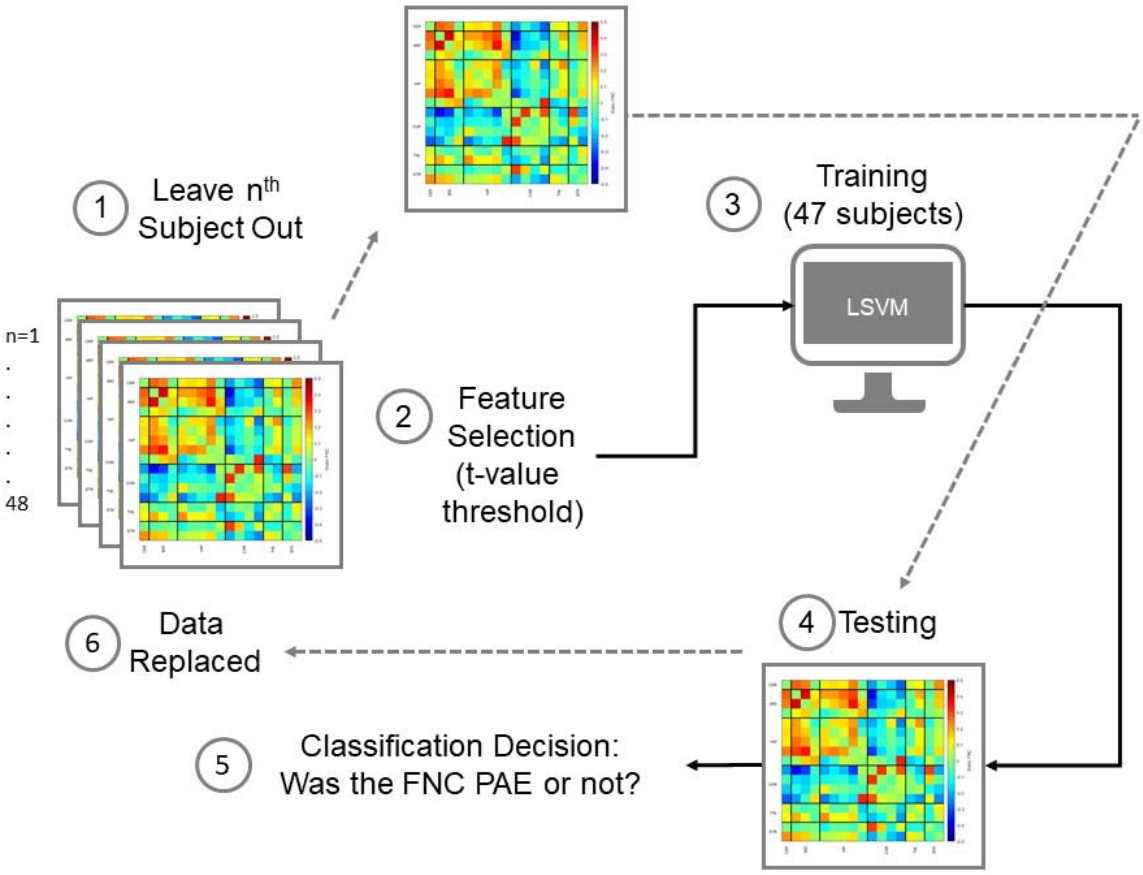

RESULTS

Retained components are displayed in Figure 2 and the anatomical location for the peak value of each component, in Paxinos and Watson space, is displayed in Table 1 (Paxinos & Watson, 2004). However, we would like to remind the reader that these components and their location were previously reported in an earlier study and do not represent results from an independent investigation. Components are displayed to aid the reader in localizing the brain regions from which the FNC measures for this study are derived from.

Table 2 displays the accuracy rates of multiple kernels used in SVM binary classification. The quadratic kernel demonstrated the highest classification rates when classifying all (both male and female samples; 62.5%) and female samples only (79.2%). The quadratic and RBF kernels demonstrated the highest accuracy rates for male samples (58.3 %). The lowest accuracy rates were observed for all samples using the RBF kernel (50%), males using the linear kernel (50%) and for females a three-way tie (66.7%) among linear, cubic, and MLP kernels. The quadratic SVM (QSVM) kernel displayed the best overall accuracy rates for discriminating between alcohol- and saccharin exposed animals and was therefore chosen for the remaining series of analyses.

253 .

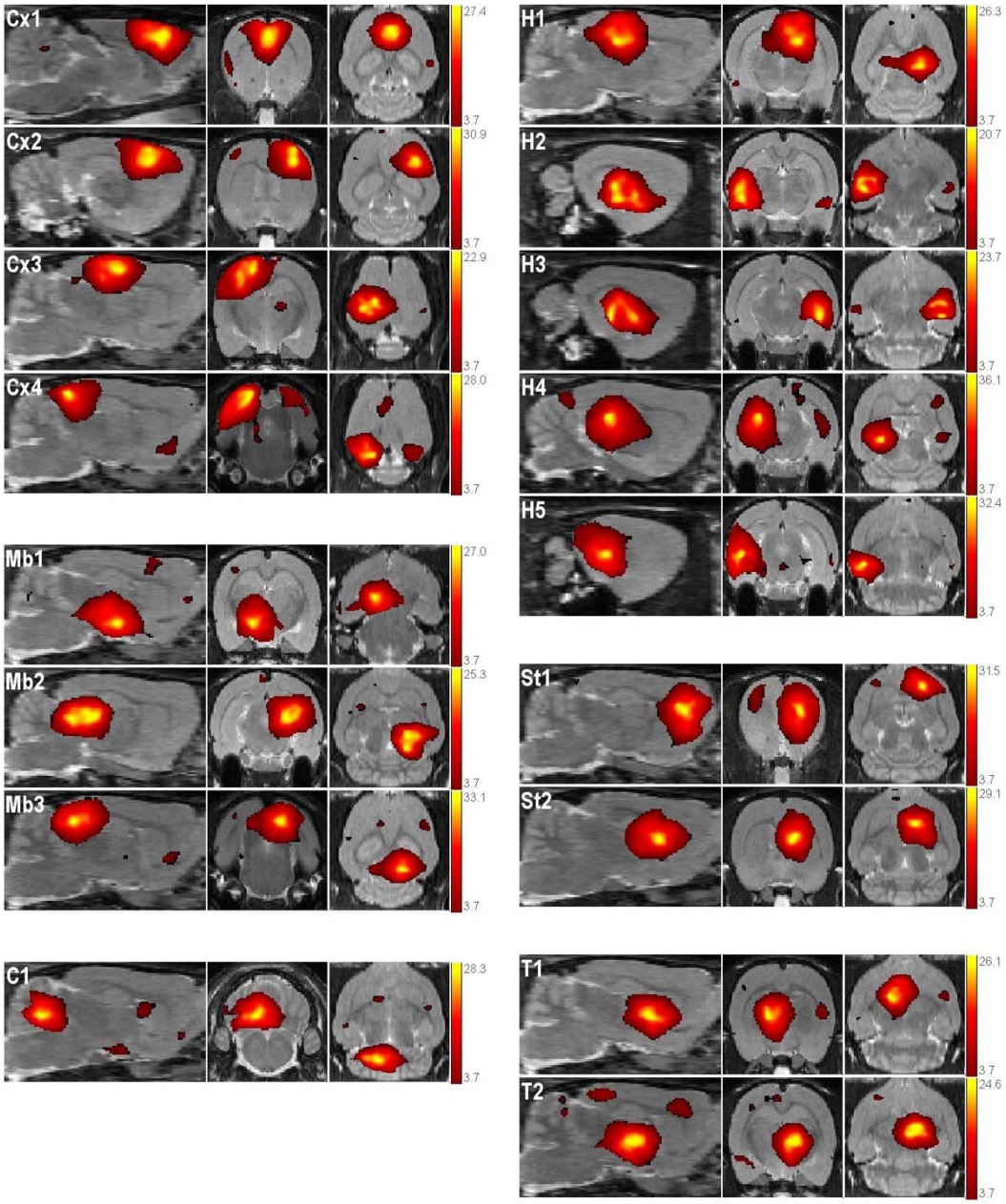

254

255 **Figure 2**. Retained independent components representing RSNs in sagittal, coronal, and axial

256 views. The anatomic location of the peak component t-value determined grouping into cortical

257 (Cx), midbrain (Mb), hippocampal (h), striatal (St), cerebellar (C) and thalamic (T) networks.

258 Reprinted with permission (Rodriguez, Davies, et al., 2016)

Table 1. Anatomical locations of extracted components. Components are arranged according to the Paxinos and Watson rat atlas (Paxinos & Watson, 2004) coordinates from anterior to posterior within regional grouping. Cortex (CX), Hippocampus (H), Midbrain (MB), Striatum (ST), and Cerebellum (C). Reprinted with permission (Rodriguez, Davies, et al., 2016).

Component Number & Label		Coordinates in (AP, ML, DV)			Abbreviation & Area	.
39	CX1	1.5	0.1	-2.7	Cg2	cingulate cortex, area 2
15	CX2	-0.1	3.5	-2.9	S1FL	primary somatosensory cortex, forelimb region
24	CX3	-3.3	-1.9	-1.5	LPtA	lateral parietal association cortex
32	CX4	-8.7	-2.1	-1.7	V2MM /V1M	secondary visual cortex, medo medial/primary visual cortex
3	H1	-5.1	2.1	-3.3	DS	dorsal subiculum
34	H2	-5.1	-5.3	-6.9	MoDG	molecular layer of the dentate gyrus
30	H3	-5.9	4.9	-6.3	Or	Oriens layer of the hippocampus
23	H4	-6.1	-3.1	-4.1	MoDG	molecular layer of the dentate gyrus
17	H5	-6.3	-5.5	-5.5	Lmol	lacunosum moleculare layer of the hippocampus
1	Mb1	-3.5	-1.9	-7.7	ZID/ZI V	zona incerta dorsal/zona incerta ventral
18	Mb2	-6.3	2.5	-4.7	InG	intermediate gray layer of the superior colliculus
6	Mb3	-8.3	1.7	-2.7	ECIC	external cortex of the inferior colliculus
14	ST1	2.1	2.3	-4.3	Cpu	Caudate Putamen
25	ST2	-0.7	1.3	-4.9	LSI	lateral septal nucleus, intermediate part

40	TH1	-1.7	-1.9	-5.9	VA/VL	region where VA and VL overlap (ventral anterior thalamic nucleus/ventrolateral thalamic nucleus)
16	TH2	-3.1	1.7	-6.1	Po	posterior thalamic nuclear group
10	C1	-11.7	-1.5	-5.1	MedDL	medial cerebellar nucleus, dorsolateral protuberance

Table 2. Classification accuracy rates of different SVM kernels. Support vector machine (SVM), radial basis (RBF), multilayer perceptron (MLP).

SVM Kernel	All Samples %	Males %	Females %
Linear	54.0	50.0	66.7
Quadratic	62.5	58.3	79.2
Cubic	60.4	41.7	66.7
RBF	50.0	58.3	70.8
MLP	54.2	54.2	66.7

Figure 3 displays accuracy-rate histograms after the prenatal conditions of FNC data were randomized and subjected to 10,000 iterations of QSVM classification and LOOCV to establish null distributions. Each null distribution was used to estimate the p=0.05 level threshold of statistical significance for accuracy rates of QSVM classification in all (A), female (B), and male samples (C). The significance threshold for all samples was 63%. Therefore, the accuracy rate for QSVM classification (62.5%) was near significance. For females, the significance threshold was estimated at 67% thus the QSVM classification rate for females (79.2%) was statistically significant. Finally, the significance threshold for males was also 67%, rendering the QSVM's performance for classifying males as not statistically significant.

A)

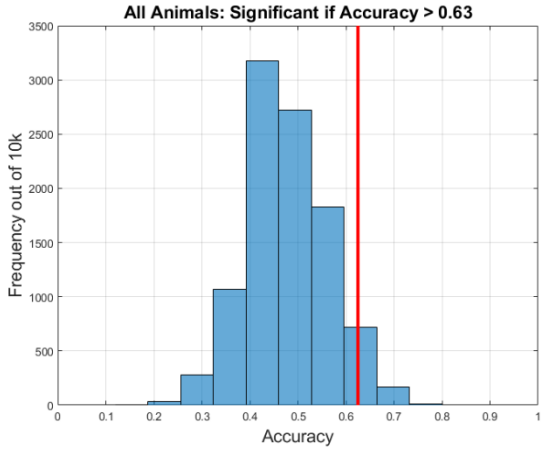

B)

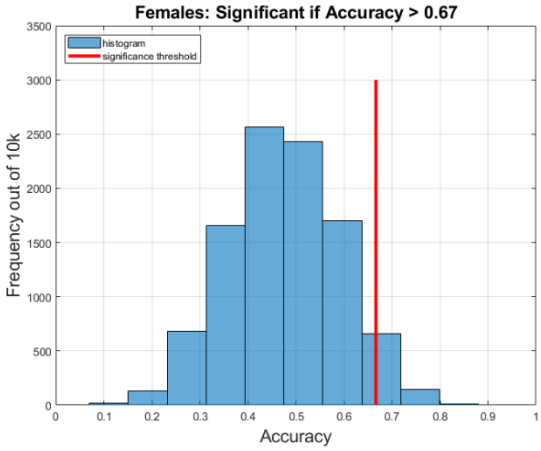

C)

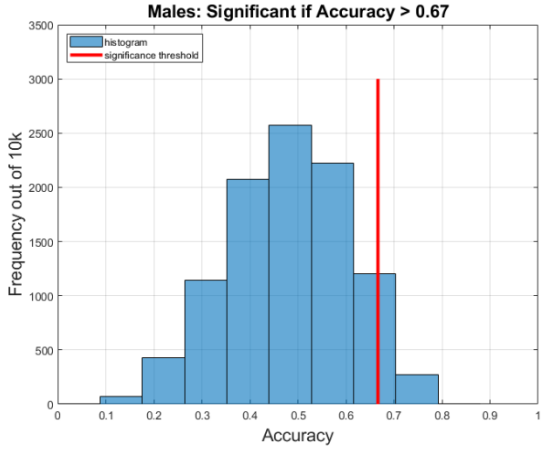

Figure 3. Null-model classification accuracy histograms illustrate the SVM classification accuracies after prenatal condition label randomization and cross validation over 10,000 iterations. The resulting distribution of accuracy rates under the null model provides the basis for calculating a *p*-value for the probability of obtaining an accuracy rate equal to or greater than observed SVM classification accuracy rates for A) All animals, B) Females, and C) Males.

The mean static FNC correlations between all independent components are displayed in Figure 4A. Moderate positive within-network connectivity (triangular regions along the diagonal) is generally observed in hippocampal, midbrain, and thalamic components while negative within network connectivity is exhibited in striatal components. Clear patterns of positive between-network connectivity are observed in midbrain-hippocampal and cerebellar-hippocampal couplings, while negative between-network connectivity is readily observed among cortical-cerebellar, cortical-midbrain, cortical-hippocampal, and cortical-thalamic couplings. Remaining combinations of connectivity display a mix of positive and negative correlations without a readily visually distinguishable pattern. Two-sample t-tests for each pairwise connectivity measure between prenatal conditions (PAE- SAC) are displayed in Figure 4B. Strong differences between conditions can be appreciated in cortical-midbrain, cortical-cortical, cortical - thalamic and cortical-striatal couplings. Separate t-test matrices for females (PAE-SAC) and males (PAE-SAC) are displayed in Figures 4C and 4D respectively. Comparing the female to male matrices reveals many of the differences from the all samples t-tests are driven by female animals. Stronger differences in mean female connectivity can be appreciated in cortical-midbrain, cortical-cortical, and cortical-striatal couplings. Less pronounced differences among male animals are generally observed with reductions in p-value magnitude readily observed in multiple regions with pronounced reductions displayed in cerebellar, cortical, and striatal networks.

A)

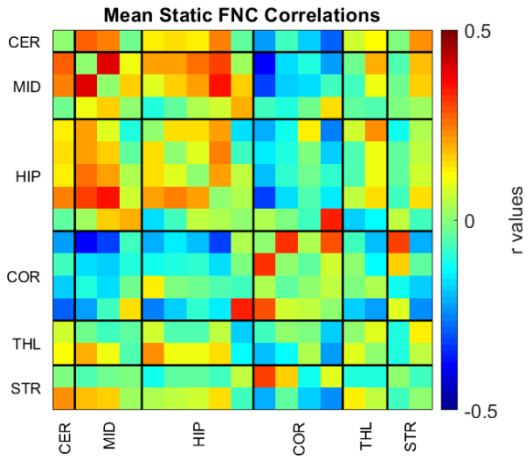

B)

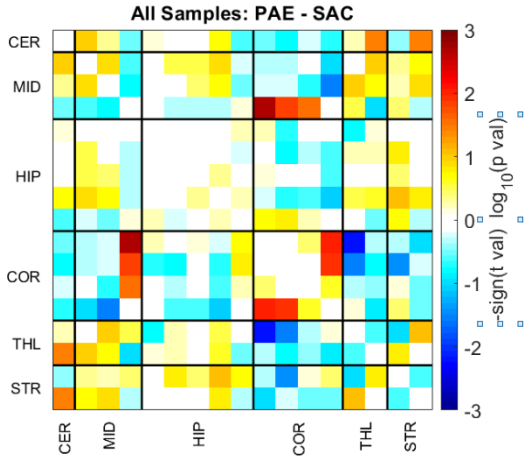

C)

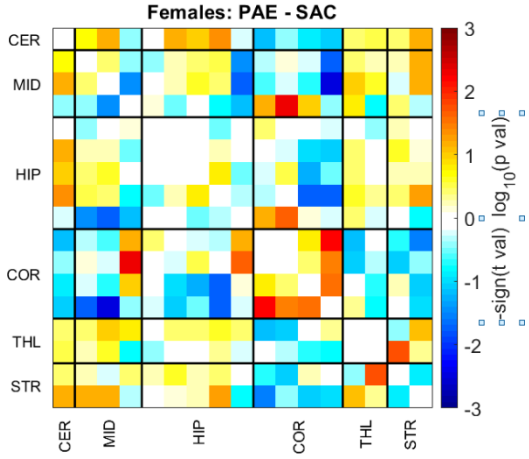

D)

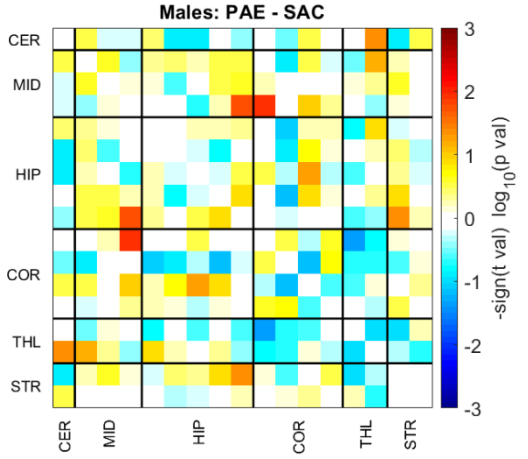

Figure 4. Mean static FNC correlation matrix for all subjects (A). Significance and direction following two-sample t-tests (PAE-SAC) on each pairwise correlation are depicted for all subjects (B), males (C) and females (D) as the -sign(t val)$\log_{10}$(p val). Component labels correspond to striatal (St), thalamic (T), cortical (Cx), hippocampal (H), midbrain (Mb), and cerebellar (C) networks.

The QSVM assigns weight to each pairwise correlation used in classification and mean classification weights are displayed in Figure 5 for all samples(A), females (B), and males (C). Weights can be used to explore the contributions of specific component correlations that most strongly impact correct classification decisions.

For all samples, a general pattern of moderately positive weights results from network correlations between cerebellar-hippocampal connectivity. Other moderate positive weights result from couplings in hippocampal-striatal, hippocampal-cortical, and hippocampal-midbrain components, while a strong mean positive weight was found in a hippocampal-thalamic coupling consisting of components with peak activations localized to the ventral-anterior thalamus and the dentate gyrus of the hippocampus. Strong negative weights result from cerebellar-cortical, hippocampal-midbrain, and cortical-striatal couplings.

For males, strong and moderately strong positive weights cluster in cortical-midbrain, cortical-hippocampal, cortical-cortical, cerebellar-hippocampal, and hippocampal-thalamic, midbrain-thalamic, midbrain-striatal, and midbrain-hippocampal connectivity. Strong negative weights are observed between striatal-cortical, cerebellar-cortical, cortical-hippocampal, and midbrain-midbrain, and striatal-thalamic connectivity.

For females, strong and moderately positive weights are observed between cortical-hippocampal, cortical-striatal, striatal-thalamic, cerebellar-hippocampal, and cerebellar-midbrain couplings. Clear patterns of moderately strong negative weights are observed in hippocampal-midbrain, cortical-cortical, cortical-cerebellar, cortical-hippocampal, cortical-cortical, thalamic-hippocampal, striatal-hippocampal, striatal-cortical, and striatal-thalamic couplings.

DISCUSSION

The motivation for this study was predicated on previous work that demonstrated regional- and sex- dependent differences in FNC patterns following moderate PAE in adult rats. Our goal was to explore the utility of machine learning to perform binary classification from resting state fMRI connectivity data acquired from an animal model of PAE. We found that a quadratic SVM kernel demonstrated the highest classification rates when compared to linear, cubic, RBF, or MLP kernels. QSVM-kernel-based classification resulted in an accuracy rate of 62.5% for all animals, 58.3% for males, and 79.2% for females. To assess statistical significance, we employed a permutation testing approach with 10,000 replications of randomization and LOOCV and found the female classification rate to surpass a $p = 0.05$ threshold. Qualitative and quantitative evaluation of FNC data and QSVM weights implicate an overarching theme of several hippocampal and cortical networks in contributing to treatment dependent differences in connectivity and the formation of correct classification decisions by the QSVM.

It is important to note that the blank cells in Figure 5 indicate correlations that did not surpass the feature selection step of the QSVM classification process. When examining these cells, a striking feature of the classification weight data is a considerable reduction in the amount of correlations used in classification of males when compared to females. Thus, a possible reason for the higher classification rate success in female animals may be due to a higher number of correlations that surpassed the t-value threshold that facilitated the classification process. These results also indicate an overall greater degree of differences in FNC across females. Interestingly, in our previous study, we found males displayed more alterations in FNC

as a result of moderate PAE (Rodriguez, Davies, et al., 2016). The present work, however, investigated non-linear data features that may be related to the improved classification of PAE in females compared to males. Another key difference for the present report is a more refined time-course pre-processing pipeline which included detrending, regression of realignment parameters, and filtering to account for in-scanner movement and to reduce the potential signal contributions stemming from respiratory processes.

Other resting state fMRI research conducted with rats exposed to prenatal alcohol has also revealed sex-dependent alterations in connectivity. Using a seed-based approach, Tang and colleagues showed baseline sex-dependent differences in functional connectivity among controls and a sex-by-alcohol interaction in cortico-striatal connectivity (Tang et al., 2019). In a subsequent investigation relying on a graph theory approach, the same research group found altered network organization in females, but not males, following PAE (Tang, Xu, Zhu, Gullapalli, & Mooney, 2020). Taken together, these findings point to the existence of sex-related differences in network connectivity in rodents with PAE with underlying mechanisms that are currently poorly understood.

Multiple reports in the literature have shown disrupted resting state functional connectivity following the administration of ketamine, a N-methyl-D-aspartate (NMDA) glutamate receptor antagonist (Grimm et al., 2015; Kraguljac et al., 2017; Motoyama et al., 2019; Mueller et al., 2018) and implicate glutamatergic neurotransmission as a candidate mechanism contributing to PAE-dependent network dysfunction. However, previous work with the same moderate PAE paradigm used in this study showed no differences in overall expression of NMDA receptors in multiple regions of the rodent

cortex (Bird et al., 2015). Moreover, while PAE-dependent increases in the expression and sensitivity of GluN2B containing NMDARs in ventrolateral frontal cortex were observed, comparisons of sex and sex-by-alcohol interactions led to null results. These findings suggest perhaps other neurotransmitter systems or physiological characteristics such as brain vascularity, may underlie sex dependent changes in connectivity after moderate PAE.

The classification technique used in this study is sparsely utilized in animal neuroimaging studies. However, investigations utilizing machine learning to detect brain dysfunction in humans from fMRI FNC data are more established. For example, a study utilizing similar methods reported an accuracy measure of 84% in correctly detecting mTBI from a static FNC data set consisting of 48 patients and 48 healthy controls (Vergara et al., 2017). A follow up investigation that utilized dynamic FNC data found a 92% accuracy measure in detecting mTBI from one of several, yet unique, connectivity states (Vergara et al., 2018).

While the performance rate for detecting PAE is not as robust as those found in human studies of mTBI, it is important to consider a set of caveats. First, maternal blood alcohol levels during prenatal development reached a moderate 60.8 mg/dL (Davies et al., 2019). In rat studies of PAE, maternal alcohol serum levels can range from 30mg/dL (Cullen, Burne, Lavidis, & Moritz, 2014) in light exposure to 300 mg/dL (Mooney & Varlinskaya, 2011) in heavier exposure models. The rodent subjects from which FNC data were acquired were exposed to levels of prenatal alcohol on the low to moderate end of the range. Second, the alcohol-exposed offspring did not produce any detectable differences in brain volume nor blood perfusion in the frontal cortex when assessed in

adulthood and compared to their respective control groups (Rodriguez, Davies, et al., 2016).

The results presented here, must also be considered within the context of a number of limitations. First, the FNC data utilized was of the static form which ignores temporal variations in connectivity across the scanning period. Examination of dynamic connectivity, which can account for these variations, may lead to disparate findings as evidenced in human-subjects research with dynamic FNC approaches showing better classification performance (Hutchison et al., 2013; Vergara et al., 2018). Future comparisons of dynamic and static FNC may reveal optimal approaches for the detection of PAE from FNC data. Furthermore, the neuroimaging data utilized to subsequently measure FNC was gathered from rodents under light isoflurane anesthesia. In our previous work, this approach was chosen to minimize the influence of motion during image acquisition. An alternative approach could employ the use of animal restraining devices to overcome anesthetic-related influences on brain function (King et al., 2005). In fact, studies conducted in rats and voles have revealed modest contributions of stress in normal and awake animals after an acclimation procedure (Liang, King, & Zhang, 2011, 2012; Reed, Pira, & Febo, 2013; Yee et al., 2016). However, changes in the sensitivity of stress-related circuitry including the hippocampus and the hypothalamic-pituitary-adrenal (HPA) axis following PAE are well documented (Hellemans, Verma, Yoon, Yu, & Weinberg, 2008; Lam, Raineki, Ellis, Yu, & Weinberg, 2018; Raineki, Ellis, & Weinberg, 2018), and carry the potential to introduce a different set of confounds in an awake scanning procedure. Next, animals in this investigation reached adulthood by the time image acquisition was conducted. Thus, additional

research will need to examine machine learning detection in earlier postnatal developmental periods to enhance any potential translational utility of this approach. Our results are based off of a total sample size of 48, and a within-sex sample size of 24 (12 PAE; 12 SAC). Consequently, the procedures employed in this report stand to benefit from validation in additional contexts with increased samples to better leverage the utility of machine learning classifiers. Finally, the fMRI data were acquired in a 3.7T scanner. Future work with higher field strength scanners (e.g. 7T or 9T) may improve signal-to-noise ratio leading to increased classification performance.

CONCLUSION

In summary, the application of support vector machine learning algorithms led to modest classification performance in discriminating alcohol-exposed from control animals utilizing FNC measures derived from the application of GICA to rodent resting state fMRI data. To our knowledge, this is the first study to apply machine learning classification methods to FNC data within the context of PAE. Future developments and refinements of the technique may lead to translational utility in human studies and lead to the development of novel and non-invasive ways of detecting FASD.

Author Contribution Statement: C.R., V.V, V.C. and D.H. conceived the presented ideas. C.R., S.D., D.S., D.H., and V.C. contributed to the previously acquired data and preprocessing. C.R., V.V., performed additional preprocessing and data analyses. Manuscript writing efforts led by C.R. and V.V. with critical feedback from all authors.

Conflict of Interest Statement: The authors of this manuscript declare no financial nor commercial relationship that could potentially serve as conflict of interests related to this research.

Support: NIH grants P30 GM103400, P50 AA022534, and R01 AA019462

REFERENCES

Allen, EA, Erhardt, EB, Damaraju, E, Gruner, W, Segall, JM, Silva, RF, . . . Calhoun, VD. A baseline for the multivariate comparison of resting-state networks. Front Syst Neurosci 2011; 5:2. doi:10.3389/fnsys.2011.00002

Arbabshirani, MR, & Calhoun, VD. Functional network connectivity during rest and task: comparison of healthy controls and schizophrenic patients. Conf Proc IEEE Eng Med Biol Soc 2011; 2011:4418-4421. doi:10.1109/IEMBS.2011.6091096

Bell, AJ, & Sejnowski, TJ. An Information Maximization Approach to Blind Separation and Blind Deconvolution. Neural Computation 1995; 7(6):1129-1159. doi:Doi 10.1162/Neco.1995.7.6.1129

Bird, CW, Candelaria-Cook, FT, Magcalas, CM, Davies, S, Valenzuela, CF, Savage, DD, & Hamilton, DA. Moderate prenatal alcohol exposure enhances GluN2B containing NMDA receptor binding and ifenprodil sensitivity in rat agranular insular cortex. PLoS One 2015; 10(3):e0118721. doi:10.1371/journal.pone.0118721

Buckner, RL, Krienen, FM, & Yeo, BT. Opportunities and limitations of intrinsic functional connectivity MRI. Nat Neurosci 2013; 16(7):832-837. doi:10.1038/nn.3423

Calhoun, VD, Adali, T, Pearlson, GD, & Pekar, JJ. A method for making group inferences from functional MRI data using independent component analysis. Hum Brain Mapp 2001; 14(3):140-151.

488 Connor, PD, Sampson, PD, Bookstein, FL, Barr, HM, & Streissguth, AP. Direct and
489 indirect effects of prenatal alcohol damage on executive function. Dev
490 Neuropsychol 2000; 18(3):331-354. doi:10.1207/S1532694204Connor
491 Cullen, CL, Burne, TH, Lavidis, NA, & Moritz, KM. Low dose prenatal alcohol exposure
492 does not impair spatial learning and memory in two tests in adult and aged rats.
493 PLoS One 2014; 9(6):e101482. doi:10.1371/journal.pone.0101482
494 Davies, S, Ballesteros-Merino, C, Allen, NA, Porch, MW, Pruitt, ME, Christensen, KH, . .
495 . Savage, DD. Impact of moderate prenatal alcohol exposure on histaminergic
496 neurons, histidine decarboxylase levels and histamine H2 receptors in adult rat
497 offspring. Alcohol 2019; 76:47-57. doi:10.1016/j.alcohol.2018.07.007
498 Gil-Mohapel, J, Boehme, F, Kainer, L, & Christie, BR. Hippocampal cell loss and
499 neurogenesis after fetal alcohol exposure: insights from different rodent models.
500 Brain Res Rev 2010; 64(2):283-303. doi:10.1016/j.brainresrev.2010.04.011
501 Green, CR, Mihic, AM, Nikkel, SM, Stade, BC, Rasmussen, C, Munoz, DP, & Reynolds,
502 JN. Executive function deficits in children with fetal alcohol spectrum disorders
503 (FASD) measured using the Cambridge Neuropsychological Tests Automated
504 Battery (CANTAB). J Child Psychol Psychiatry 2009; 50(6):688-697.
505 doi:10.1111/j.1469-7610.2008.01990.x
506 Grimm, O, Gass, N, Weber-Fahr, W, Sartorius, A, Schenker, E, Spedding, M, . . .
507 Meyer-Lindenberg, A. Acute ketamine challenge increases resting state
508 prefrontal-hippocampal connectivity in both humans and rats.
509 Psychopharmacology (Berl) 2015; 232(21-22):4231-4241. doi:10.1007/s00213-
510 015-4022-y

Hamilton, DA, Magcalas, CM, Barto, D, Bird, CW, Rodriguez, CI, Fink, BC, . . . Savage, DD. Moderate Prenatal Alcohol Exposure and Quantification of Social Behavior in Adult Rats. Jove-Journal of Visualized Experiments 2014; (94). doi:ARTN e52407

10.3791/52407

Hellemans, KG, Verma, P, Yoon, E, Yu, W, & Weinberg, J. Prenatal alcohol exposure increases vulnerability to stress and anxiety-like disorders in adulthood. Ann N Y Acad Sci 2008; 1144:154-175. doi:10.1196/annals.1418.016

Hutchison, RM, Womelsdorf, T, Allen, EA, Bandettini, PA, Calhoun, VD, Corbetta, M, . . . Chang, C. Dynamic functional connectivity: promise, issues, and interpretations. Neuroimage 2013; 80:360-378. doi:10.1016/j.neuroimage.2013.05.079

Jones, KL, & Smith, DW. Recognition of the fetal alcohol syndrome in early infancy. Lancet 1973; 302(7836):999-1001.

Jones, KL, & Smith, DW. The fetal alcohol syndrome. Teratology 1975; 12(1):1-10. doi:10.1002/tera.1420120102

King, JA, Garelick, TS, Brevard, ME, Chen, W, Messenger, TL, Duong, TQ, & Ferris, CF. Procedure for minimizing stress for fMRI studies in conscious rats. J Neurosci Methods 2005; 148(2):154-160. doi:10.1016/j.jneumeth.2005.04.011

Kraguljac, NV, Frolich, MA, Tran, S, White, DM, Nichols, N, Barton-McArdle, A, . . . Lahti, AC. Ketamine modulates hippocampal neurochemistry and functional connectivity: a combined magnetic resonance spectroscopy and resting-state fMRI study in healthy volunteers. Mol Psychiatry 2017; 22(4):562-569. doi:10.1038/mp.2016.122

534 Lam, VYY, Raineki, C, Ellis, L, Yu, W, & Weinberg, J. Interactive effects of prenatal
535 alcohol exposure and chronic stress in adulthood on anxiety-like behavior and
536 central stress-related receptor mRNA expression: Sex- and time-dependent
537 effects. Psychoneuroendocrinology 2018; 97:8-19.
538 doi:10.1016/j.psyneuen.2018.06.018
539 Lemoine, P, Harousseau, H, Borteyru, JP, & Menuet, JC. Children of Alcoholic Parents -
540 Anomalies in 127 Cases. Archives Francaises De Pediatrie 1968; 25(7):830-+.
541 Retrieved from <Go to ISI>://WOS:A1968B838800015
542 Liang, Z, King, J, & Zhang, N. Uncovering intrinsic connectional architecture of
543 functional networks in awake rat brain. J Neurosci 2011; 31(10):3776-3783.
544 doi:10.1523/JNEUROSCI.4557-10.2011
545 Liang, Z, King, J, & Zhang, N. Anticorrelated resting-state functional connectivity in
546 awake rat brain. Neuroimage 2012; 59(2):1190-1199.
547 doi:10.1016/j.neuroimage.2011.08.009
548 Logothetis, NK, Pauls, J, Augath, M, Trinath, T, & Oeltermann, A. Neurophysiological
549 investigation of the basis of the fMRI signal. Nature 2001; 412(6843):150-157.
550 doi:10.1038/35084005
551 Loock, C, Conry, J, Cook, JL, Chudley, AE, & Rosales, T. Identifying fetal alcohol
552 spectrum disorder in primary care. CMAJ 2005; 172(5):628-630.
553 doi:10.1503/cmaj.050135
554 Manning, MA, & Eugene Hoyme, H. Fetal alcohol spectrum disorders: a practical clinical
555 approach to diagnosis. Neurosci Biobehav Rev 2007; 31(2):230-238.
556 doi:10.1016/j.neubiorev.2006.06.016

557 Mattson, SN, & Riley, EP. A review of the neurobehavioral deficits in children with fetal
558 alcohol syndrome or prenatal exposure to alcohol. Alcohol Clin Exp Res 1998;
559 22(2):279-294.
560 May, PA, Baete, A, Russo, J, Elliott, AJ, Blankenship, J, Kalberg, WO, . . . Hoyme, HE.
561 Prevalence and characteristics of fetal alcohol spectrum disorders. Pediatrics
562 2014; 134(5):855-866. doi:10.1542/peds.2013-3319
563 May, PA, Chambers, CD, Kalberg, WO, Zellner, J, Feldman, H, Buckley, D, . . . Hoyme,
564 HE. Prevalence of Fetal Alcohol Spectrum Disorders in 4 US Communities.
565 Jama-Journal of the American Medical Association 2018; 319(5):474-482.
566 doi:10.1001/jama.2017.21896
567 May, PA, & Gossage, JP. Estimating the prevalence of fetal alcohol syndrome. A
568 summary. Alcohol Res Health 2001; 25(3):159-167.
569 Mooney, SM, & Varlinskaya, EI. Acute prenatal exposure to ethanol and social
570 behavior: effects of age, sex, and timing of exposure. Behavioural Brain
571 Research 2011; 216(1):358-364. doi:10.1016/j.bbr.2010.08.014
572 Motoyama, Y, Oshiro, Y, Takao, Y, Sato, H, Obata, N, Izuta, S, . . . Kan, S. Resting-
573 state brain functional connectivity in patients with chronic pain who responded to
574 subanesthetic-dose ketamine. Sci Rep 2019; 9(1):12912. doi:10.1038/s41598-
575 019-49360-1
576 Mueller, F, Musso, F, London, M, de Boer, P, Zacharias, N, & Winterer, G.
577 Pharmacological fMRI: Effects of subanesthetic ketamine on resting-state
578 functional connectivity in the default mode network, salience network, dorsal

attention network and executive control network. Neuroimage Clin 2018; 19:745-757. doi:10.1016/j.nicl.2018.05.037

Patten, AR, Fontaine, CJ, & Christie, BR. A comparison of the different animal models of fetal alcohol spectrum disorders and their use in studying complex behaviors. Front Pediatr 2014; 2:93. doi:10.3389/fped.2014.00093

Paxinos, G, & Watson, C. (2004). *The Rat Brain in Stereotaxic Coordinates - The New Coronal Set* (5th ed.): Academic Press.

Popova, S, Stade, B, Bekmuradov, D, Lange, S, & Rehm, J. What do we know about the economic impact of fetal alcohol spectrum disorder? A systematic literature review. Alcohol Alcohol 2011; 46(4):490-497. doi:10.1093/alcalc/agr029

Raichle, ME, & Mintun, MA. Brain work and brain imaging. Annu Rev Neurosci 2006; 29:449-476. doi:10.1146/annurev.neuro.29.051605.112819

Raineki, C, Ellis, L, & Weinberg, J. Impact of adolescent stress on the expression of stress-related receptors in the hippocampus of animals exposed to alcohol prenatally. Hippocampus 2018; 28(3):201-216. doi:10.1002/hipo.22823

Rashid, B, Arbabshirani, MR, Damaraju, E, Cetin, MS, Miller, R, Pearlson, GD, & Calhoun, VD. Classification of schizophrenia and bipolar patients using static and dynamic resting-state fMRI brain connectivity. Neuroimage 2016; 134:645-657.

Reed, MD, Pira, AS, & Febo, M. Behavioral effects of acclimatization to restraint protocol used for awake animal imaging. J Neurosci Methods 2013; 217(1-2):63-66. doi:10.1016/j.jneumeth.2013.03.023

600 Rodriguez, CI, Davies, S, Calhoun, V, Savage, DD, & Hamilton, DA. Moderate Prenatal
601 Alcohol Exposure Alters Functional Connectivity in the Adult Rat Brain. Alcohol
602 Clin Exp Res 2016; 40(10):2134-2146. doi:10.1111/acer.13175
603 Rodriguez, CI, Magcalas, CM, Barto, D, Fink, BC, Rice, JP, Bird, CW, . . . Hamilton, DA.
604 Effects of sex and housing on social, spatial, and motor behavior in adult rats
605 exposed to moderate levels of alcohol during prenatal development. Behavioural
606 Brain Research 2016; 313:233-243. doi:10.1016/j.bbr.2016.07.018
607 Savage, DD, Becher, M, de la Torre, AJ, & Sutherland, RJ. Dose-dependent effects of
608 prenatal ethanol exposure on synaptic plasticity and learning in mature offspring.
609 Alcohol Clin Exp Res 2002; 26(11):1752-1758.
610 doi:10.1097/01.ALC.0000038265.52107.20
611 Schweinhardt, P, Fransson, P, Olson, L, Spenger, C, & Andersson, JL. A template for
612 spatial normalisation of MR images of the rat brain. J Neurosci Methods 2003;
613 129(2):105-113.
614 Servais, L, Hourez, R, Bearzatto, B, Gall, D, Schiffmann, SN, & Cheron, G. Purkinje cell
615 dysfunction and alteration of long-term synaptic plasticity in fetal alcohol
616 syndrome. Proc Natl Acad Sci U S A 2007; 104(23):9858-9863.
617 doi:10.1073/pnas.0607037104
618 Snyder, AZ, & Raichle, ME. A brief history of the resting state: the Washington
619 University perspective. Neuroimage 2012; 62(2):902-910.
620 doi:10.1016/j.neuroimage.2012.01.044
621 Streissguth, AP, Barr, HM, Sampson, PD, Parrishjohnson, JC, Kirchner, GL, & Martin,
622 DC. Attention, Distraction and Reaction-Time at Age 7 Years and Prenatal

623 Alcohol Exposure. Neurobehavioral Toxicology and Teratology 1986; 8(6):717-
624 725. Retrieved from <Go to ISI>://WOS:A1986F500000016
625 Streissguth, AP, Bookstein, FL, Barr, HM, Sampson, PD, O'Malley, K, & Young, JK.
626 Risk factors for adverse life outcomes in fetal alcohol syndrome and fetal alcohol
627 effects. Journal of Developmental and Behavioral Pediatrics 2004; 25(4):228-
628 238. doi:Doi 10.1097/00004703-200408000-00002
629 Tang, S, Xu, S, Waddell, J, Zhu, W, Gullapalli, RP, & Mooney, SM. Functional
630 Connectivity and Metabolic Alterations in Medial Prefrontal Cortex in a Rat Model
631 of Fetal Alcohol Spectrum Disorder: A Resting-State Functional Magnetic
632 Resonance Imaging and in vivo Proton Magnetic Resonance Spectroscopy
633 Study. Dev Neurosci 2019; 41(1-2):67-78. doi:10.1159/000499183
634 Tang, S, Xu, S, Zhu, W, Gullapalli, RP, & Mooney, SM. Alterations in the whole brain
635 network organization after prenatal ethanol exposure. Eur J Neurosci 2020;
636 51(10):2110-2118. doi:10.1111/ejn.14653
637 Vergara, VM, Mayer, AR, Damaraju, E, Kiehl, KA, & Calhoun, V. Detection of Mild
638 Traumatic Brain Injury by Machine Learning Classification Using Resting State
639 Functional Network Connectivity and Fractional Anisotropy. Journal of
640 Neurotrauma 2017; 34(5):1045-1053. doi:10.1089/neu.2016.4526
641 Vergara, VM, Mayer, AR, Kiehl, KA, & Calhoun, VD. Dynamic functional network
642 connectivity discriminates mild traumatic brain injury through machine learning.
643 Neuroimage Clin 2018; 19:30-37. doi:10.1016/j.nicl.2018.03.017
644 Williams, JF, Smith, VC, & Committee On Substance, A. Fetal Alcohol Spectrum
645 Disorders. Pediatrics 2015. doi:10.1542/peds.2015-3113

Yee, JR, Kenkel, WM, Kulkarni, P, Moore, K, Perkeybile, AM, Toddes, S, . . . Ferris, CF. BOLD fMRI in awake prairie voles: A platform for translational social and affective neuroscience. Neuroimage 2016; 138:221-232. doi:10.1016/j.neuroimage.2016.05.046